frontiers | Frontiers in Computer Science

TYPE Original Research
PUBLISHED 12 October 2022
DOI 10.3389/fcomp.2022.990290

OPEN ACCESS

EDITED BY
Upal Mahbub,
Qualcomm, United States

REVIEWED BY
Bo Lei,
Xi'an University of Post and Telecommunications, China
Jörg Miehling,
Friedrich-Alexander-Universität Erlangen-Nürnberg, Germany

*CORRESPONDENCE
Huang Chao
chao@szu.edu.cn

SPECIALTY SECTION
This article was submitted to Computer Vision, a section of the journal Frontiers in Computer Science

RECEIVED 09 July 2022
ACCEPTED 26 September 2022
PUBLISHED 12 October 2022

CITATION
Luximon A, Chao H, Goonetilleke RS and Luximon Y (2022) Theory and applications of InfraRed and thermal image analysis in ergonomics research. *Front. Comput. Sci.* 4:990290. doi: 10.3389/fcomp.2022.990290

Theory and applications of InfraRed and thermal image analysis in ergonomics research

Ameersing Luximon[1], Huang Chao[2]*, Ravindra S. Goonetilleke[3] and Yan Luximon[4]

[1]Industrial Design Department, Georgia Tech Shenzhen Institute (GTSI), Shenzhen, China, [2]Art Division, Shenzhen University, Shenzhen, China, [3]Department of Industrial and Systems Engineering, Khalifa University, Abu Dhabi, United Arab Emirates, [4]Asian Ergonomics Design, School of Design, The Hong Kong Polytechnic University, Kowloon, Hong Kong SAR, China

Designing products and services to fit human needs, wants and lifestyle require meaningful data. With Industry 4.0 and the internet of things, we have many ways to capture data using sensors and other means. InfraRed (IR) cameras are quite ubiquitous, especially for screening illness and wellness. They can provide a wealth of data on different objects and even people. However, their use has been limited due to processing complexities. With reducing cost and increasing accuracy of IR cameras, access to thermal data is becoming quite widespread, especially in medicine and people-related applications. These cameras have software to help process the data, with a focus on qualitative analyses and rather primitive quantitative analyses. In ergonomics, data from multiple users are essential to make reasonable predictions for a given population. In this study, using 4 simple experiments, several quantitative analysis techniques such as simple statistics, multivariate statistics, geometric modeling, and Fourier series modeling are applied to IR images and videos to extract essential user and population data. Results show that IR data can be useful to provide user and population data that are important for design. More research in modeling IR data and application software is needed for the increased application of IR information in ergonomics applications.

KEYWORDS

ergonomics, thermal models, InfraRed images, InfraRed video, multivariate analysis, Industry 4.0, heat mapping, thermal camera

Introduction

Although clinical thermometry, defined as the use of temperature measurements for both diagnostic and health monitoring is longstanding, practical radiometric determination of human body temperature started with the development of the Evaporograph in 1925 by Prof Marianus Czerny (Ring, 2012). Later, with the development of Pyroscan (Cade and Barlow, 1967), the first British medical thermograph was obtained during World War II. Even though revolutionary, it was slow and not so detailed in comparison to today's equipment. For example, a one-hand thermogram using the Pyroscan took around 5 min, and the temperature was represented in black and white in the thermogram. Even though thermography was rudimentary, its use in medical settings started to emerge with thousands of thermography scans per year

on females to rule out breast-related diseases (Gershon-Cohen, 1967). After the 1960s, rapid developments took place and now modern IR thermal imaging is fast and accurate with applications in many fields (Kirimtat et al., 2020). IR thermography systems have progressed fast due to improvements in sensors, diagnostic procedures, computing power and improved processing algorithms (Faust et al., 2014).

IR thermography is a very promising method for evaluating variations in skin temperature, and signs of potential disease or disorders in the human body (Skomudek et al., 2017; Kirimtat et al., 2020). Thus, it is no surprise that IR thermal imaging is now widely used in medical settings (Faust et al., 2014). Some of them include identifying scoliosis (Kwok et al., 2017), facial paralysis (Liu et al., 2021), diabetic foot (Macdonald et al., 2016; Cruz-Vega et al., 2020; van Doremalen et al., 2020), breast cancer and tumors (Kakileti et al., 2020; Resmini et al., 2021), and sprain injuries (Oliveira et al., 2016). Cardone and Merla (2017) have shown that thermal imaging can also be used for the assessment of human autonomic nervous activity and psychophysiological states by measuring pulse rate, breathing rate, cutaneous blood perfusion, sudomotor response, stress response, and social interactions. Other applications include those in sports science related to injury prevention, detection of sports injuries, injury follow-up, physical and emotional load evaluations, and design of sports equipment and clothing (Hildebrandt et al., 2010; Quesada, 2017; Drzazga et al., 2018). Although the applications of IR thermography are growing rapidly, many challenges remain, especially in the analysis and interpretation of the data collected.

When an IR image is captured, it does not differentiate between the region of interest (ROI) and the background. Various techniques have been used to capture the ROI, either manually or automatically, depending on the distance between the IR equipment and the participant (Barcelos et al., 2014; Quesada, 2017; Perpetuini et al., 2021). After obtaining the necessary images, qualitative and quantitative approaches are used for their interpretation. Current analysis methods are rather conservative (Quesada et al., 2017). Qualitative analysis of IR thermography data involves color-coded image representation with different temperature ranges superimposed on normal RGB images as a heat map (Quesada et al., 2017); and mapping IR images onto a 3D human body model (Chao et al., 2015). When considering quantitative analysis, average temperature, maximum temperature, temperature variation, standard deviation, thermal symmetries, and thermal gradients are used based on the ROI (Quesada et al., 2017).

Processing images of one participant can be straightforward, but with multiple participants of differing weight, height and BMI, obtaining meaningful results can be challenging. Multivariate statistical analysis techniques such as PCA, factor analysis and cluster analysis are some possible techniques that can be used to group and classify data (Timm, 2002). IR cameras provide not just thermograms (images), but also videos. Analysis of videos is also challenging when considering variations between different people with the added time-related variations. Very few studies have considered the different parts of the body and analysis of the video IR data of the human body. Statistical analysis of human data and representation of these data in an efficient manner can provide enormous value as a new source of knowledge and information for product designers.

In order to address this challenge, we describe four experiments that cover the head and face, hands, feet and the whole body. The objectives are:

1. Extract suitable metrics to analyze IR data so that useful standards may be generated.
2. Process the images and video of more than one participant so that more general recommendations can be made. Multidimensional scaling (Luximon and Luximon, 2009; Chao et al., 2015), multivariate statistical analysis (Timm, 2002), and Fourier series modeling (Stade, 2011) will be used to extract useful information from IR images and videos.

The main contribution of the paper is to show the use statistical analysis, mathematical analysis, time series analysis, image, and video data analysis based on IR data. Similar techniques can be applied to new IR data set for create database for different age group, Body Mass Index (BMI), gender, and cultures. In addition, heat signatures (or heat map) for different diseases can be identified for medical intervention. Additional research in this area is needed to develop standards for thermograms for different body parts at different settings. Based on differences in heat map different products and situations can be evaluated (Luximon et al., 2016). Results from

TABLE 1 Setting of different experiments.

Experiment	Focus	IR equipment	Environment setting
1	Leg	FLIR E33	Temperature 23°C, relative humidity 30%
2	Face	FLIR E33	Temperature 24°C, relative humidity 60%
3	Hand	FLIR E33	Temperature 23°C, relative humidity 30%
4	Whole body	FLIR A6700sc	Temperature 24°C, relative humidity 60%

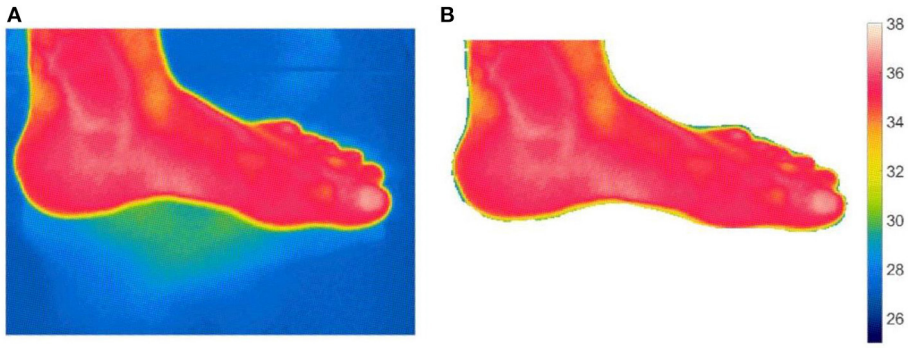

C

n	R	G	B	n	R	G	B	n	R	G	B	n	R	G	B	n	R	G	B	n	R	G	B
1	229	232	226	31	240	48	81	61	250	150	22	91	212	214	16	121	14	143	134	151	0	75	184
2	250	220	194	32	244	44	82	62	246	158	14	92	199	213	6	122	9	141	156	152	1	73	176
3	251	221	195	33	238	38	76	63	248	160	17	93	191	204	0	123	8	140	155	153	0	70	173
4	252	219	184	34	238	33	75	64	249	166	14	94	185	205	0	124	2	139	168	154	0	69	166
5	249	216	182	35	237	32	74	65	251	168	17	95	180	199	0	125	2	139	168	155	0	68	165
6	250	209	177	36	248	26	74	66	252	172	15	96	184	211	2	126	0	136	179	156	3	65	158
7	244	203	172	37	247	25	72	67	253	174	16	97	174	201	0	127	0	136	179	157	2	64	157
8	244	194	166	38	252	22	65	68	244	180	13	98	173	204	0	128	0	130	202	158	2	61	148
9	239	189	160	39	251	21	64	69	248	184	17	99	172	203	0	129	0	129	201	159	0	59	146
10	245	180	156	40	246	24	58	70	244	183	12	100	151	203	0	130	0	128	203	160	1	56	138
11	242	178	154	41	247	25	59	71	249	187	17	101	148	199	0	131	0	128	203	161	0	54	135
12	249	167	149	42	244	31	50	72	245	192	14	102	145	199	5	132	0	121	220	162	0	51	131
13	247	165	147	43	245	32	51	73	246	193	15	103	142	197	3	133	0	121	220	163	0	50	130
14	251	156	142	44	243	37	59	74	242	197	12	104	127	192	4	134	0	119	221	164	4	44	131
15	246	150	137	45	248	42	64	75	242	197	12	105	124	189	1	135	0	116	218	165	2	43	129
16	248	140	131	46	252	43	59	76	239	202	10	106	112	186	13	136	6	115	219	166	3	39	125
17	242	134	125	47	255	46	62	77	239	202	10	107	108	181	9	137	4	112	217	167	0	36	122
18	242	129	124	48	249	62	50	78	235	206	5	108	97	181	30	138	0	106	219	168	0	30	113
19	239	126	121	49	248	61	49	79	235	206	5	109	93	177	26	139	0	107	220	169	0	26	109
20	251	112	115	50	247	69	29	80	232	208	3	110	79	175	36	140	9	95	221	170	0	23	101
21	249	109	113	51	255	77	37	81	232	208	3	111	77	172	33	141	8	94	220	171	0	20	99
22	247	103	110	52	244	88	41	82	230	210	1	112	69	171	50	142	0	99	208	172	0	14	91
23	243	98	106	53	250	94	46	83	230	210	1	113	66	167	47	143	0	96	205	173	0	13	90
24	243	89	100	54	248	100	39	84	226	211	9	114	59	161	67	144	0	90	205	174	4	10	83
25	239	84	95	55	251	104	42	85	228	213	11	115	56	157	64	145	0	87	202	175	0	6	79
26	241	77	94	56	252	120	37	86	218	209	0	116	35	162	96	146	0	83	196	176	2	2	73
27	239	75	91	57	255	125	42	87	225	216	5	117	33	159	94	147	0	83	196	177	0	0	71
28	243	63	90	58	251	134	28	88	217	212	4	118	26	152	121	148	4	82	192	178	1	0	67
29	237	57	84	59	255	139	33	89	220	215	8	119	22	148	117	149	3	81	191	179	0	0	66
30	240	48	81	60	249	149	21	90	206	209	10	120	15	144	135	150	3	79	188	180	0	0	69
																				181	0	1	73

FIGURE 1
Extracting data from an IR image and video. **(A)** IR image from camera. **(B)** IR image after removing background. **(C)** Colormap values to convert video frame images to index image ($n = 181$).

this type of study will be useful to create design tools for product designers.

Materials and methods

Experiments 1, 2 and 3 used a FLIR E33 IR Camera (FLIR USA) while a FLIR A6700sc Camera (FLIR USA) was used in experiment 4. In experiment 1 and 3, the temperature of the room was around 23°C (SD = 1°C) and relative humidity was around 30% (SD = 9%). In experiment 2 and 4, the indoor room temperature was around 24 ± 1°C and relative humidity was around 60 ± 5%. Digital temperature-humidity recorder, testo 175 H1—Temperature and humidity data logger was used to

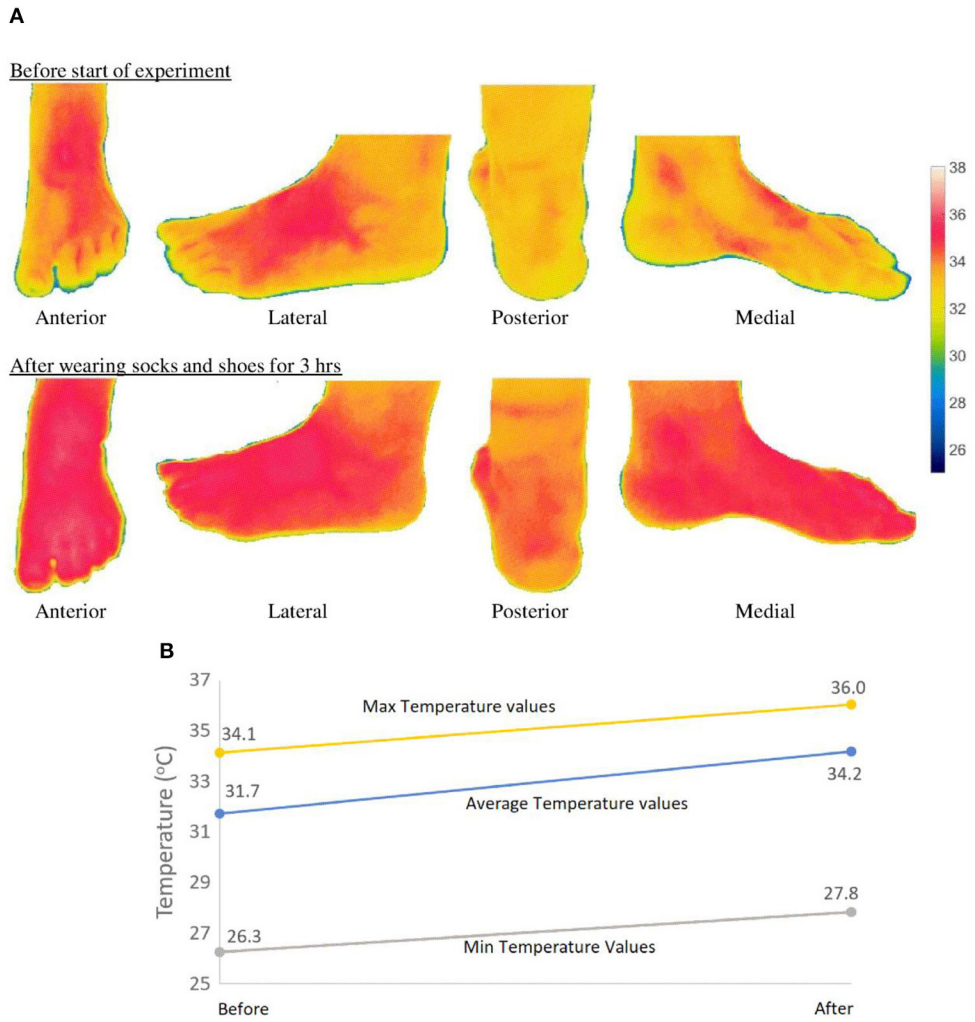

FIGURE 2
Temperature (°C) distribution on the foot. **(A)** Plots of temperature (°C) distribution on foot surface. **(B)** Plots of mean values of all participants the min, average and maximum temperature values (before and after).

TABLE 2 Analysis of variance.

Source	Sum sq.	d.f.	Mean sq.	F	Prob > F
Before-after	95.003	1	95.0026	152.59	0
Left-right	0.694	1	0.6936	1.11	0.2943
Position	8.799	3	2.9331	4.71	0.0044
Before-after* left-right	0.4	1	0.4004	0.64	0.4249
Before-after* position	0.109	3	0.0362	0.06	0.9815
Left-right* position	0.049	3	0.0164	0.03	0.9942
Error	51.674	83	0.6226		
Total	156.728	95			

*Interaction.

monitor in real time the relative humidity and indoor air temperature.

All participants were assessed by a registered physiotherapist for any abnormalities and infections. None of the participants had any. The experiment was approved by the University Ethics committee (HSEARS20141209003). An informed consent form was obtained from each subject. In experiment 1, six female Hong Kong of south Asian origin of mean age of 43 years (SD = 10 years) participated (Luximon et al., 2017). The IR camera was placed at a fixed position and subjects positioned their feet on a paper template pasted on the floor. The IR images of four views (anterior, posterior, medial and lateral position) were captured at the start of the experiment (i.e., before). The participants then wore socks and shoes for 3 h.

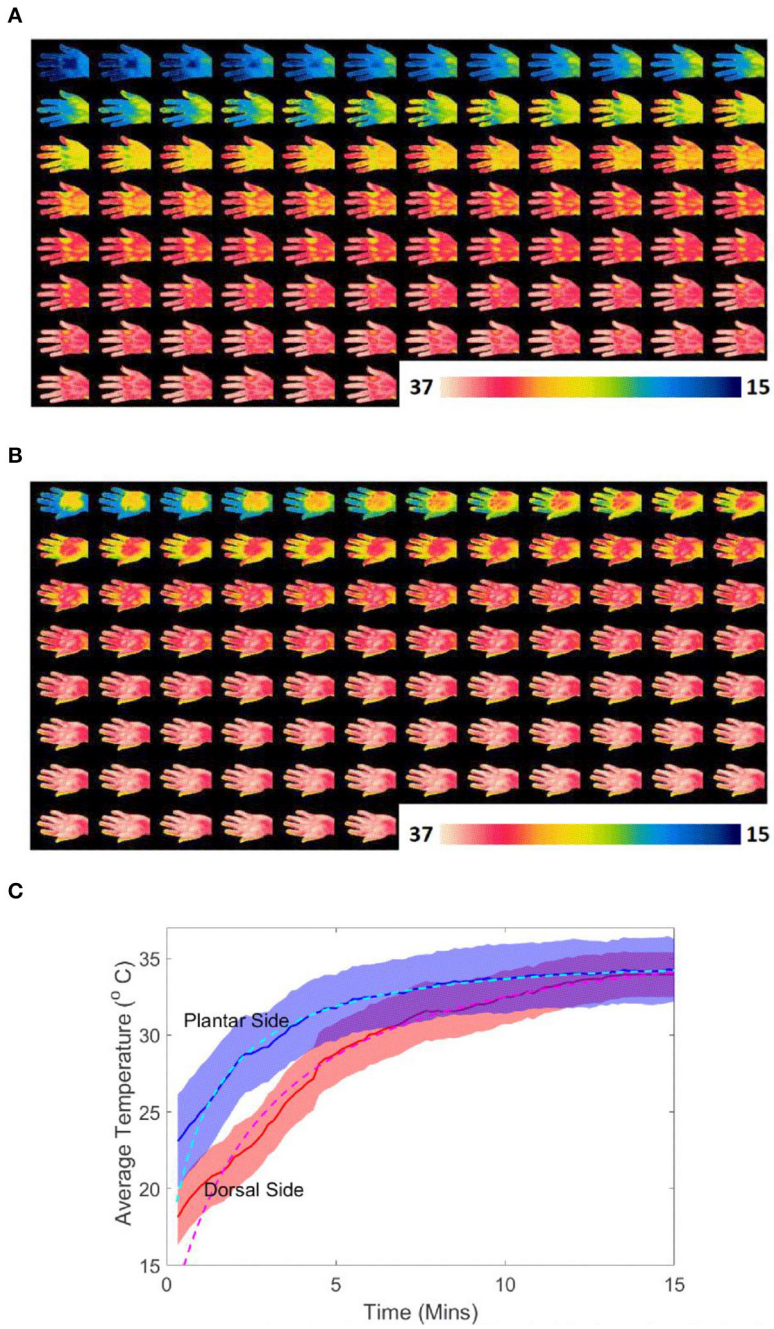

FIGURE 3
Temperature on the dorsal and plantar sides of the hand after dipping hand in ice cold water for 1 min. **(A)** Thermal images of the dorsal side of the hand after dipping hand in ice cold water for 1 min (total time = 15 min, time interval 10 s). **(B)** Thermal images of the plantar side of the hand after dipping hand in ice cold water for 1 min (total time = 15 min, time interval 10 s). **(C)** Average temperature on dorsal and planter side of hand with time after dipping hand in ice cold water for 1 min (shaded shows the ±SD range).

The socks were provided to the participant and they were the same type for all participants. Then the IR images of the 4 views were captured after removing the shoes and socks (i.e., after).

In experiment 2, the IR video of one Chinese participant aged 30 years (height 182 cm, and weight 82 kg) was collected when wearing two types of face masks. The face masks were a 3M N95 respirator from 3M Korea Ltd. and a surgical

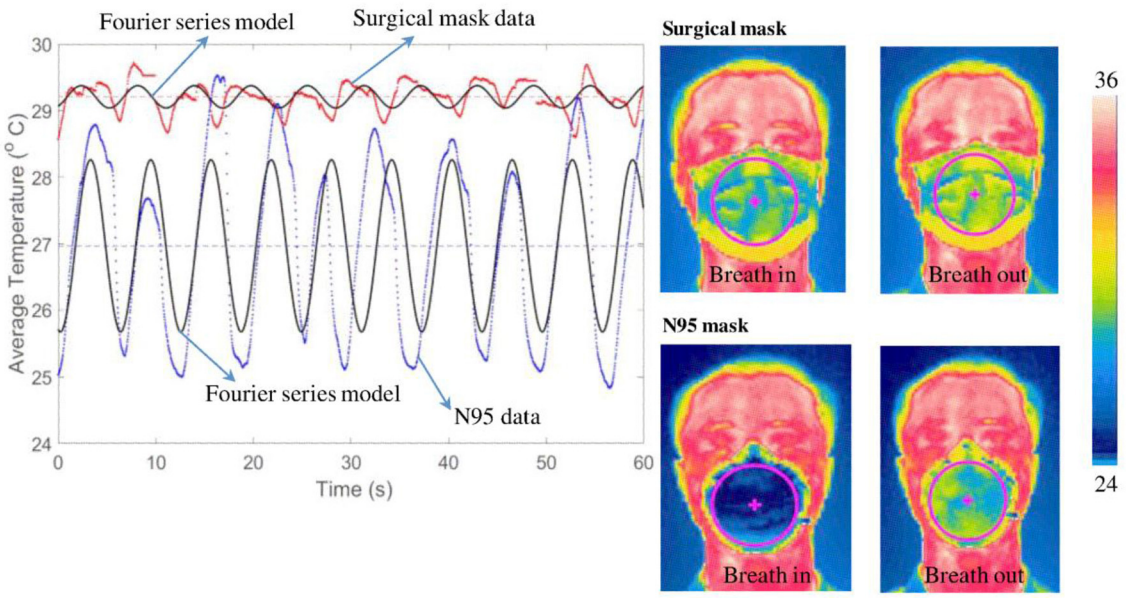

FIGURE 4
Mean temperature variation over time when wearing different face masks.

TABLE 3 Coefficients of the Fourier series model.

n	n^*w	w	a_0	a_1	b_1	a_2	b_2	a_3	b_3
N95									
1	1.02	1.02	26.97	−1.25	−0.31	1.02			
2	1.02	0.51	26.96	−0.19	0.34	−1.25	−0.33	0.51	
3	1.01	0.34	26.97	0.24	0.17	−0.66	−0.28	−1.24	−0.15
Surgical mask									
1	1.08	1.08	29.21	−0.14	0.09	1.08			
2	1.08	0.54	29.21	−0.01	−0.04	−0.14	0.10	0.54	
3	1.08	0.36	29.21	−0.03	0.00	−0.01	0.05	−0.13	0.10

mask from US Secure Co. Ltd. A video was recorded at 30 frames per second. For experiment 3, the IR video from one Hong Kong participant of south Asian origin aged 52 years (height 165 cm, and weight 75 kg) was collected after the hand was submerged in ice-cold water (0°C). The left hand was submerged in ice-cold water for 1 min, the hand was dried, and was placed at a fixed location. A thermal video, of the dorsal side of the hand, was recorded at 30 frames per second. After 30 min, the procedure was repeated to capture data from the plantar side of the same hand. In experiment 4, the front and back of the whole body were scanned of 15 healthy Chinese male participants whose mean age was 21.4 years (SD = 2.1 years), mean height was 172 cm (SD = 8 cm), mean weight was 63 kg (SD = 11 kg), mean BMI was 21.2 (SD = 3.2).

A summary of the setting is shown in Table 1.

Analysis and results

Data from the IR Camera were images and video. The IR images were converted into actual temperature values and exported into a .csv format using FLIR software tools. In this study, the background data was manually removed from the IR images. The unwanted background was set to be transparent, and the IR images were saved as png files. An image mask was used to extract the accurate temperature data from the .csv file (Figures 1A,B). Unlike the images, the extracted images from the videos cannot be converted directly into temperature values. Using the color-coded temperature scale and the color information from the video frames, the temperature data of each frame was extracted using programs written in Matlab. The RGB images extracted from the video data were converted into an indexed image ($I_1 \Rightarrow$ High temperature and $I_n \Rightarrow$ Low temperature, where $n = 181$) using the colormap shown in Figure 1C. The indexed values (I_k) in the images were then converted into temperature values (T_k) based on the minimum (T_{Min}) and maximum (T_{Max}) of the temperature scale using Equation (1). Since the conversion of the video color-coded data to temperature values is dependent on the temperature scale setting, it is important to set the correct temperature

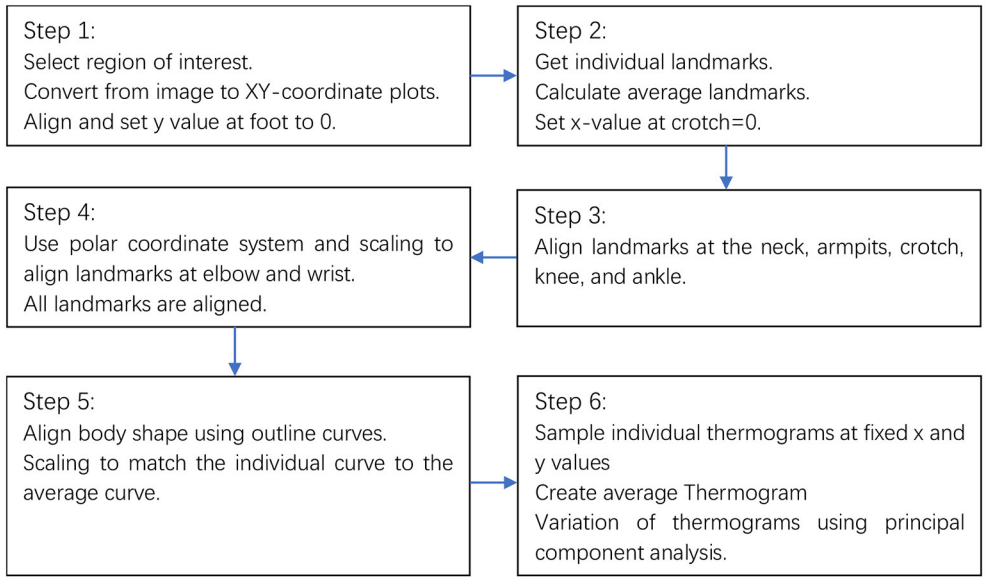

FIGURE 5
Flow chart for the analysis.

range to capture the temperature changes. This requires trial and error and a series of pilot experiments. All the model development and analysis were performed using programs written in Matlab.

$$T_k = \frac{(T_{\max} - T_{Min})}{(I_1 - I_n)} (I_k - I_n) + T_{Min} \quad (1)$$

Experiment 1: Foot IR data

In experiment 1, IR mages were acquired, and the temperature data was obtained by converting the IR images to a .csv temperature data file. Figure 2 shows the temperature distribution of the left foot when viewed from the anterior, lateral, posterior, and medial sides before and after wearing socks and shoes. After removing the background information, the foot was the ROI. The minimum, maximum and average and standard deviation of the temperature of each participant for the left and right foot and the 4 sides were calculated. The analysis of variance (ANOVA) (Table 2) showed significant differences in average temperature before and after wearing socks and shoes [$F_{(1,83)} = 152$, $p < 0.05$] and also the different views of the foot [$F_{(3,83)} = 4.71$, $p < 0.05$]. The mean average temperature before wearing socks was 32°C and after wearing socks and shoes it was 34°C. The mean average temperature of the front view was higher than the temperature of the posterior view by 0.8°C. There were no statistical differences among the other views. Figure 2B shows a plot of the minimum, maximum and average temperature values before and after wearing socks and shoes. The average temperature of the foot is higher after wearing socks and shoes for 3 h.

Experiment 2: Hand IR data

The aim of experiment 2 was to demonstrate the use of qualitative and time-domain analysis. In experiment 2, video data was acquired from the IR camera. Figure 3A shows the thermograms of the dorsal side of the hand after submerging the hand in ice-cold water for 1 min. Figure 3B shows the thermograms of the plantar side of the hand after submerging the hand in ice-cold water for 1 min. The thermograms show the temperature changes at 10 s intervals over a total time of 15 min. For qualitative as well as quantitative analysis of IR video data, the setting of the minimum temperature and maximum temperature values of the color-coded temperature scale is important. Several trials were carried out to decide on the minimum temperature (= 15°C) and maximum temperature (37°C) values of the color-coded temperature scale. If the minimum temperature is set to lower values, then the hand will appear "white" after a few minutes. If the minimum temperature is set to a higher value, then the venous structures of the hand will not be very visible. Thus, the maximum temperature was set to 37°C, as the normal body temperature

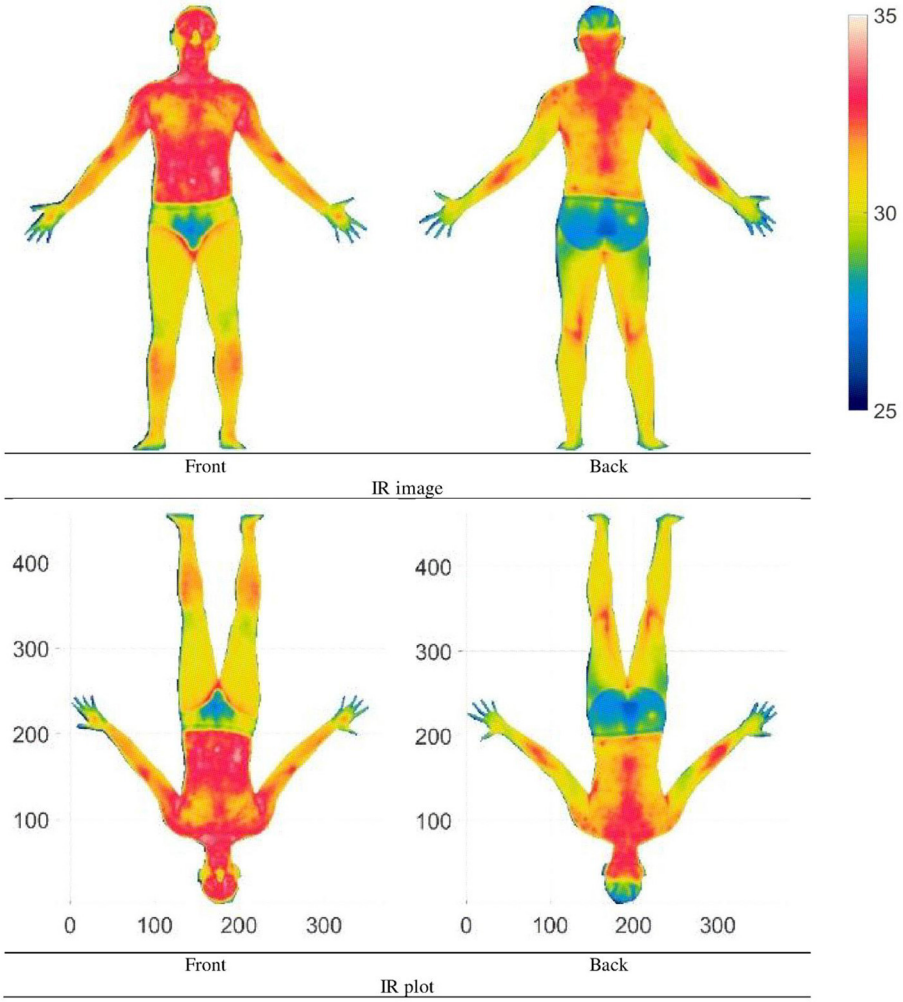

FIGURE 6
Whole-body IR image of an individual (Units: Pixel).

is around 37°C. An image mask at a selected time frame (T = 20 s) was used to remove the background data. During data recording, the hand was still, and hence using one image mask was sufficient to remove the background from all images in the video.

In Figure 3A, when the hand warms up, the dorsal venous network is visible. In health screenings, the rate of change of temperature and the heat contours can provide important information about blood flow. From Figures 3A,B, it can be seen that the dorsal side is colder than the plantar side when putting the hand in cold water for the same amount of time. On the plantar side, the venous network is not clear. This is due to the difference in dorsal and plantar hand anatomy. The variation of the average temperature on the dorsal (red line) and plantar side (blue line) of the hand, over time, after submerging the hand in ice-cold water for 1 min (shaded shows the ±SD range) is shown in Figure 3C. The figure also shows the trend as a dotted line. The equations corresponding to the temperature trend line of the dorsal and plantar sides (T_{Dorsal} and $T_{Plantar}$) are given in Equations (2) and (3), respectively.

$$T_{Dorsal} = 37 - \frac{1}{\left(0.0004t^2 + 0.0144t + 0.0379\right)}, \; R^2 = 0.9913 \tag{2}$$

$$T_{Plantar} = 37 - \frac{1}{\left(0.0009t^2 + 0.0343t + 0.0457\right)}, \; R^2 = 0.9961 \tag{3}$$

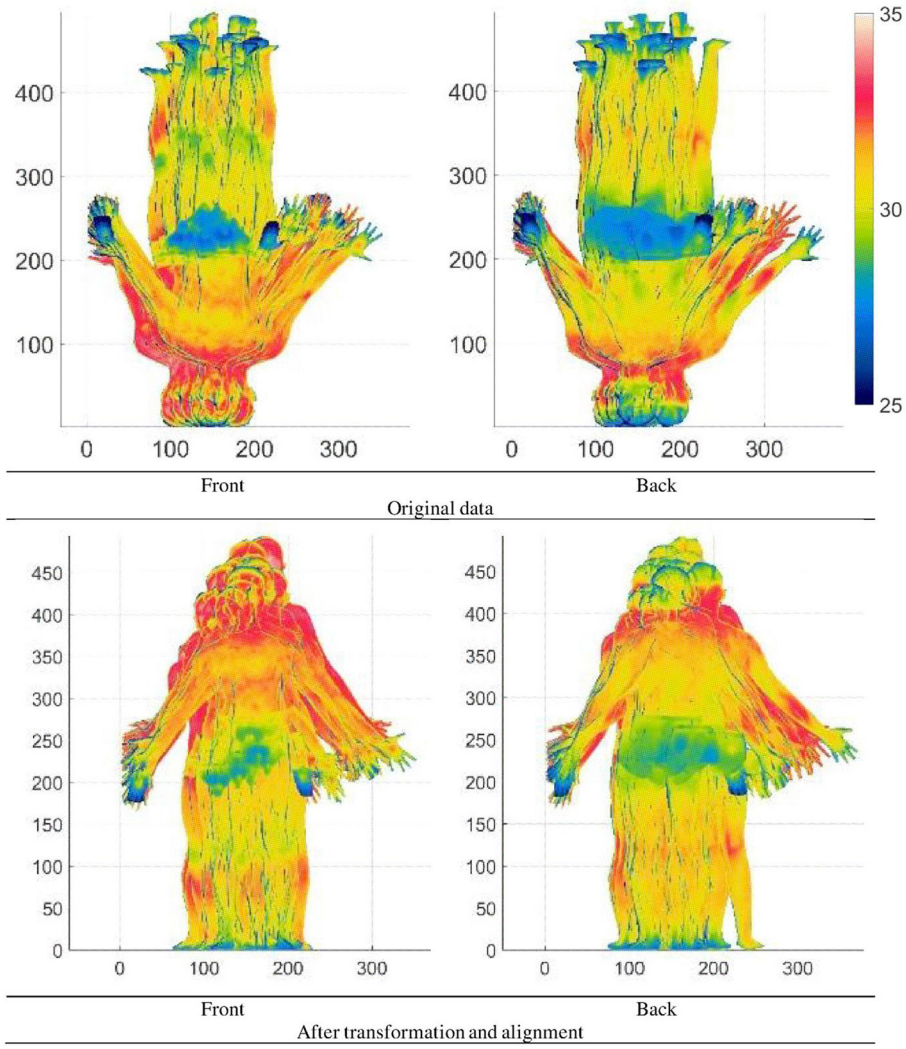

FIGURE 7
Whole-body IR plots of all participants (Units: Pixel).

Experiment 3: Head IR data

In experiment 3, video data was acquired from an IR camera. The temperature values were extracted based on a color-coded temperature scale (minimum temperature value 24°C and maximum temperature value 36°C). A circular region of radius 25 pixels was selected. The circle and the center of the circle is shown in Figure 4. The IR data was collected for about 20 min, but for this paper, we present only a selected portion (1 min) to analyze the breathing cycle. Figure 4 also shows instances of the IR temperature when breathing in and breathing out using two face masks. The time series plot for the mean temperature values in the selected circular region is shown in Figure 4. Since the time series data shows periodicity, the data was modeled using Fourier series. The general formula of the Fourier series is given in Equation (4). T is the average time of the selected circular region and t is the time in seconds. a_0, a_i, bi and w are model constants. The Fourier series model was developed using non-linear least squares estimation and was computed in Matlab. The fourier series model was developed using Non-linear Least Squares estimation model and was computed in Matlab. The Curve Fitting Toolbox of Matlab is needed and the function "*fit*" with Fourier Series Model Names (fourier1, fourier2, fourier3, ...) was used. The values for the coefficient of the models are shown in Table 3, when $n = 1$, 2, and 3. If we consider $n = 1$, for N95 face mask Fourier series model, the values and the 95% confidence bound for the constants are: $a_0 = 26.97$ (26.92, 27.01), $a_1 = -1.25$ (−1.32, −1.18),

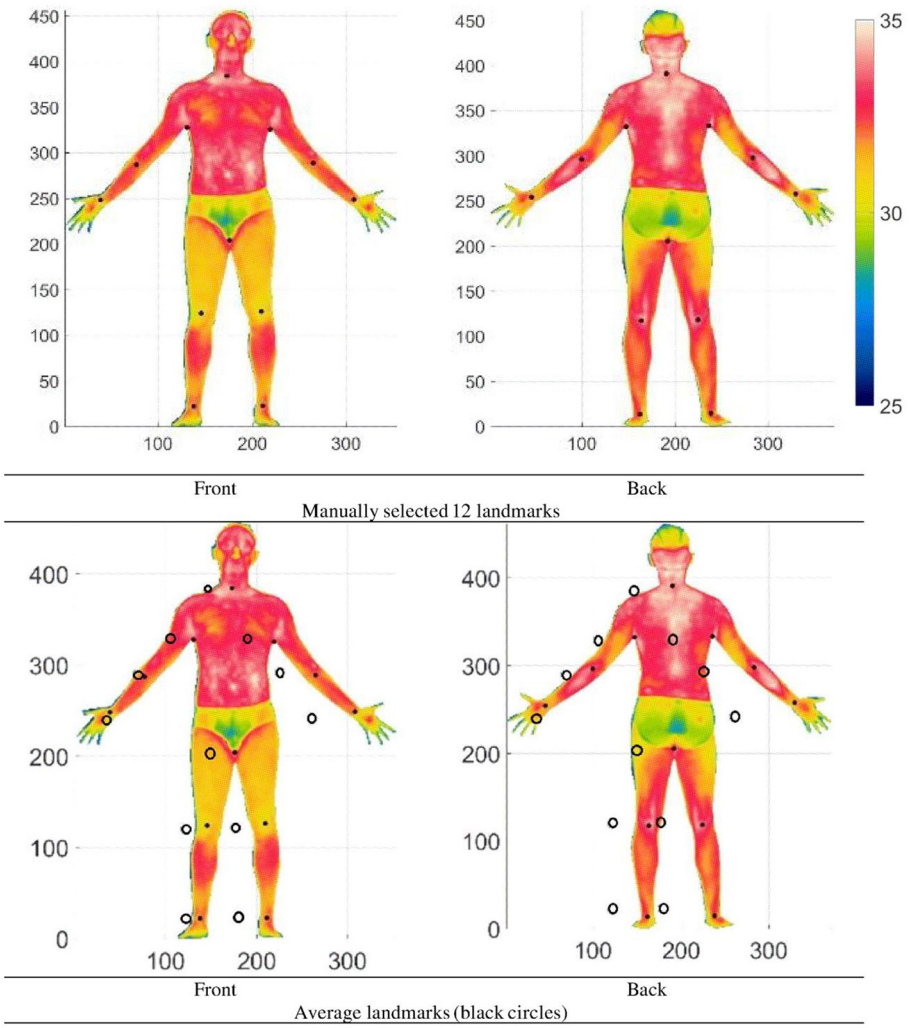

FIGURE 8
The 12 landmarks and the average of the landmarks (Units: Pixel).

$b_1 = -0.31$ (−0.43, −0.18) and w = 1.02 (1.02, 1.02). For the surgical mask fourier series model, the mean values and the 95% confidence bounds for the constants are: $a_0 = 29.21$ (29.20, 29.21), $a_1 = -0.14$ (−0.16, −0.12), $b_1 = 0.09$ (0.07, 0.11) and w = 1.08 (1.08, 1.09). It can be seen from Figure 4, that the average temperature of the surgical mask (≈29°C) is higher than the N95 mask (≈27°C). The breathing cycle period is given by 2*pi/w. For the N95 face mask, the mean value and the 95% confidence bounds for the period are 6.17 s [6.15 6.19]. For the surgical mask, the mean value and the 95% confidence bounds for the period are 5.79 s [5.77 5.82]. The study shows that different types of masks can affect the breathing rate.

For the surgical mask, the breathing rate = 60/5.7928 ≈ 10 breaths per minute, and for the N95 mask, the breathing rate = 60/6.17 = 9.7 breaths per minute. This experiment illustrates the application of a Fourier series model for IR data analysis.

$$T = a_0 + \sum_{i=1}^{n} a_i \cos(iwt) + b_i \sin(iwt) \quad (4)$$

Experiment 4: Whole body IR data

The different steps for analyzing the whole body are shown in the flow chart Figure 5.

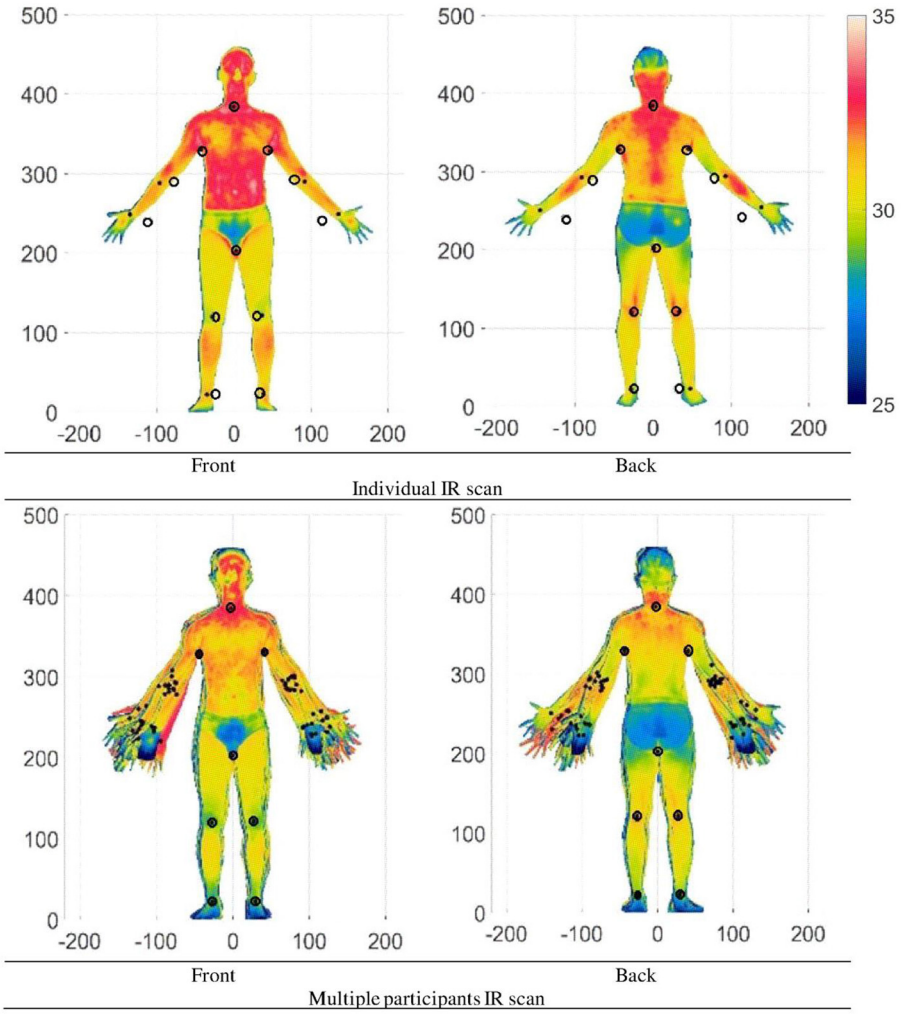

FIGURE 9
IR plots after matching the x and y values at the neck, armpits, crotch, knee, and ankle (Units: Pixel).

Step 1

The IR images for one participant and the XY surface plots (x and y units are in pixels) are shown in Figure 6. The IR data points i for participant j and side k (front or back) is given by point P_{ijk} with coordinates $(x_{ijk}, y_{ijk})|$ where $i = 1,\ldots, N_{jk}$; $j = 1,\ldots, 15$; and $k = 1,\ldots, 2$. N_{jk} is the number of data points for participants j and side k. The plots of all the data are shown in Figure 7. Rotations and translations were used to transform participants' data into an upright position as shown in Figure 7.

Step 2

Landmarks are the way to register multiple images. These reference landmarks can be added either automatically or manually. In this paper, 12 landmarks were manually selected (crotch (L_{Crotch}), ankle [positive side ($_PL_{Ankle}$) and Negative side ($_NL_{Ankle}$)], positive and negative side of knee ($_PL_{Knee}$ and $_NL_{Knee}$), positive and negative side of Armpit ($_PL_{Arm}$ and $_NL_{Arm}$), positive and negative side of elbow ($_PL_{Elbow}$ and $_NL_{Elbow}$), positive and negative side of wrist ($_PL_{Wrist}$ and $_NL_{Wrist}$) and neck (L_{Neck}). The landmarks are shown in Figure 8. The landmark i for participant j and side k (front or back) is given by point L_{ijk} with coordinates ($_Lx_{ijk}$, $_Ly_{ijk}$) where $i = 1,\ldots, 12$; $j = 1,\ldots, 15$; and k = 1,…, 2. The mean points of the landmarks are then calculated. The average landmark i for side k is given by point $_ALik$ with coordinates ($_{AL}x_{ik}$, $_{AL}y_{ik}$) where $i = 1,\ldots, 12$; and k = 1,…, 2. For one participant, the individual and average landmarks are shown in Figure 8. The average landmarks are represented by black

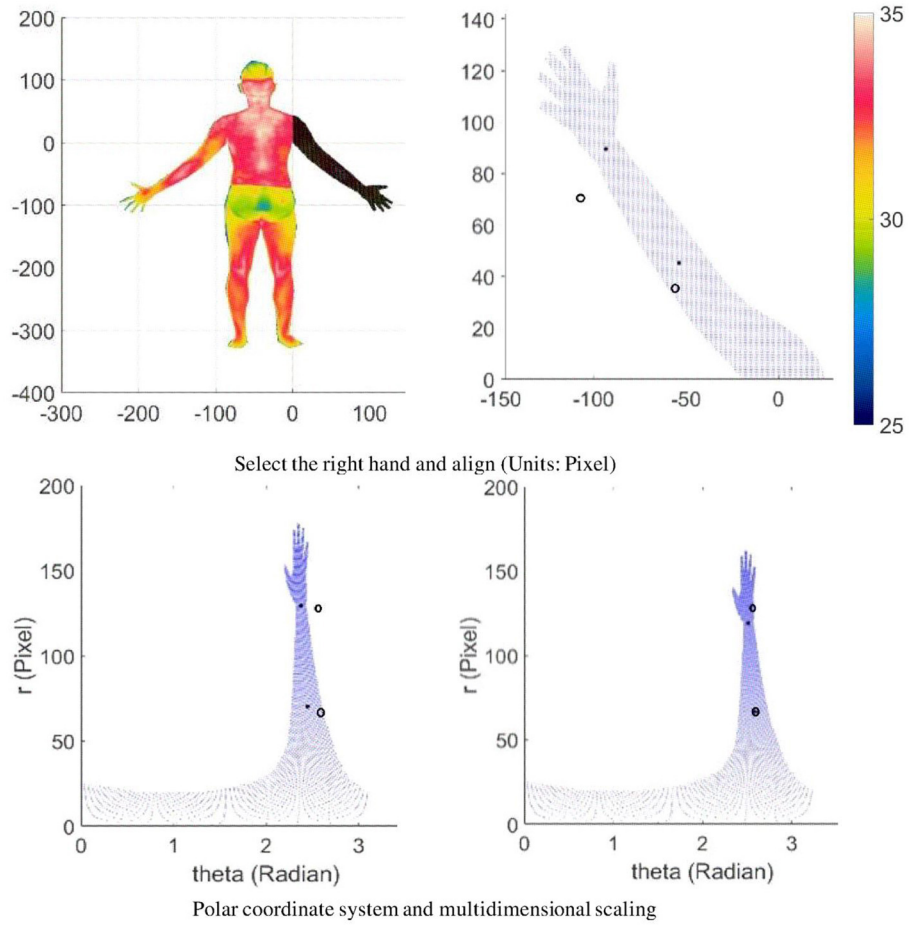

FIGURE 10
Hand in the polar coordinate system followed by multidimensional scaling to match landmark at the elbow.

circles, while the individual landmarks are represented by black dots.

Step 3

The individual IR data is first matched at the neck landmark. Then IR data is multidimensionally scaled (Luximon and Luximon, 2009; Chao et al., 2015) to match the individual x and y values of the landmarks at the armpits, crotch, knees and ankles to the x and y of the average respective landmarks as shown in Figure 9. If the y-value of an average landmark is y_{LA} and the y-value of individual landmark is y_{LI} all the points between y = 0 to y_{LI} can be scaled by a scale factor y_{LA}/y_{LI}. By scaling different sections between the landmarks and scaling in x and y direction, the landmarks are matched. This is basically the multidimensional scaling technique.

Step 4

IR data is transformed to match the individual x and y values of the landmarks (elbows and wrists) to the average x and y values of the landmarks (elbows and wrists). To do this, we used polar coordinate transformation (use matlab code cart2pol) with the arm pit landmark as reference point and then multidimensional shear and scaling to match the landmarks at the elbow (Figure 10). If the xy-value of an average landmark is (x_{LA}, y_{LA}) and the xy-value of individual landmark is (x_{LI}, y_{LI}) and y_{LA}= y_{LI}. The difference in x-value at y_{LA} is $dx = x_{LA} - x_{LI}$. For any individual points (x_i, y_i) using shear transformation, $x_i = x_i + y_i^* dx / y_{LA}$. When considering selected region and the center point, shear can be applied to deform the shape. The location of the center point Figure 10 (right image) is at the center of the arm pit to the shoulder position. The value can be adjusted to provide accurate and realistic deformation. The elbow was used as a reference to match the wrist using multidimensional shear and scaling.

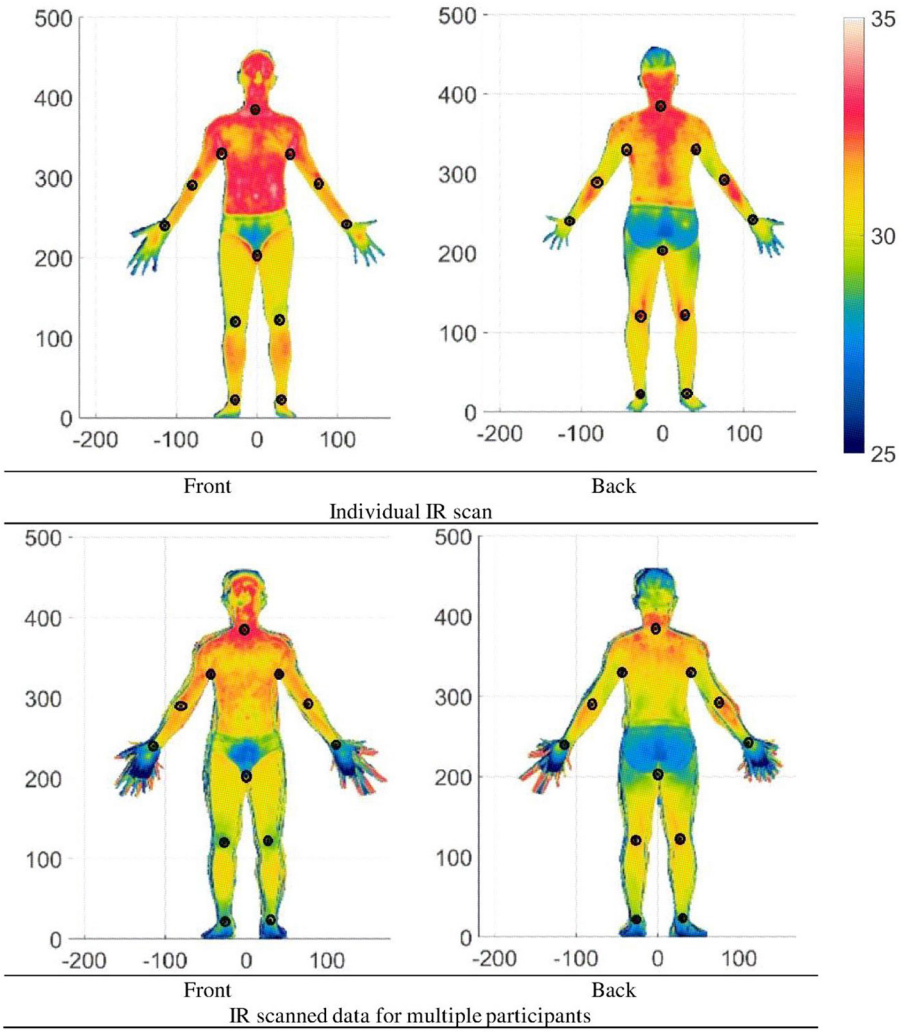

FIGURE 11
IR scanned data after matching all landmarks (Units: Pixel).

Figure 11 shows the plots of an individual and plots of all the participants, respectively.

Step 5

The whole-body IR data has potential applications in the design of functional clothing, hence the extremities such as the hand, feet and head data were not used. Generally, if the hand, head and feet are the ROI, then accurate data of these extremities are separately obtained. Figure 12 shows the plots of all the participants' data without the head and extremities. Although the data looks aligned and overlapped, due to different body types, the outline of the shapes does not match exactly. To match the shape of all participants exactly, 8 outline curves (C_i where $i = 1,\ldots, 8$) are extracted. As an example, the curves C_1 of all participants are shown and the average of the curves is calculated and plotted (in red) as shown in Figure 13. Using the outlines as a guide, the IR data are scaled using multidimensional scaling to match the average outline curves (Figure 13).

Step 6

Although the IR data are bounded by the average outline curves, the number of data points is not the same for different participants. For statistical analysis such as principal component analysis (PCA) (matlab function pca), the IR data were uniformly sampled to have the same number of data points for all participants. After sampling the mean and mean $\pm$ SD of the IR data based on all participants are shown

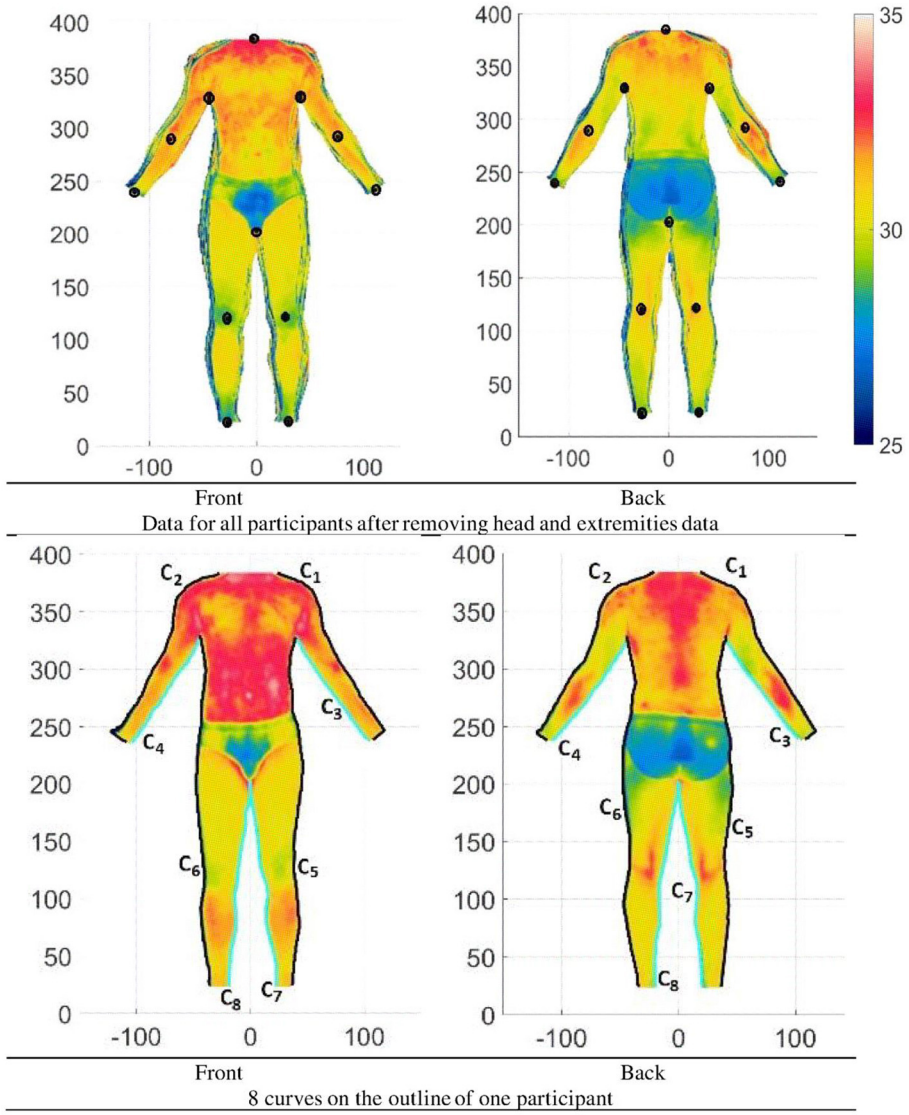

FIGURE 12
Whole-body IR scanned data after matching all landmarks and removing head and extremities data and extracting outline curves (Units: Pixel).

in Figure 14. Using the sampled data principal component analysis is carried out. The results of the first 4 principal components (PC_i where $i = 1,\ldots, 4$) are shown in Figures 15, 16 for the back and front sides of the human body. From Figures 15, 16, it can be seen that PC_1 is related to the IR distribution of the whole body. When PC_1 is low, the temperature of the whole body is low and vice versa. From Figure 15, it can be seen that the PC_2 of the back side of the whole body is somewhat related to the IR distribution of the extremities and torso. In general, with increasing PC_2 values, the temperature of the extremities increases and the temperature of the torso decreases. PC_3 is somewhat related to the IR distribution of the leg. With increasing PC_3 values the temperature of the leg decreases. PC_4 is somewhat related to the IR distribution of the upper arm and leg. In general, with increasing PC_4 values the temperature of the upper arm and leg decreases. From Figure 16, it can be seen that the PC_2 of the back side of the whole body is somewhat related to the IR distribution of the leg. In general, with increasing PC_2 values, the temperature of the leg increases. PC_3 is somewhat related to the IR distribution of the arm and lower leg. In general, with increasing PC_3 values, the temperature of the arms increases, and those of the lower leg decrease. PC_4 is somewhat related to the IR distribution of the upper leg. In general,

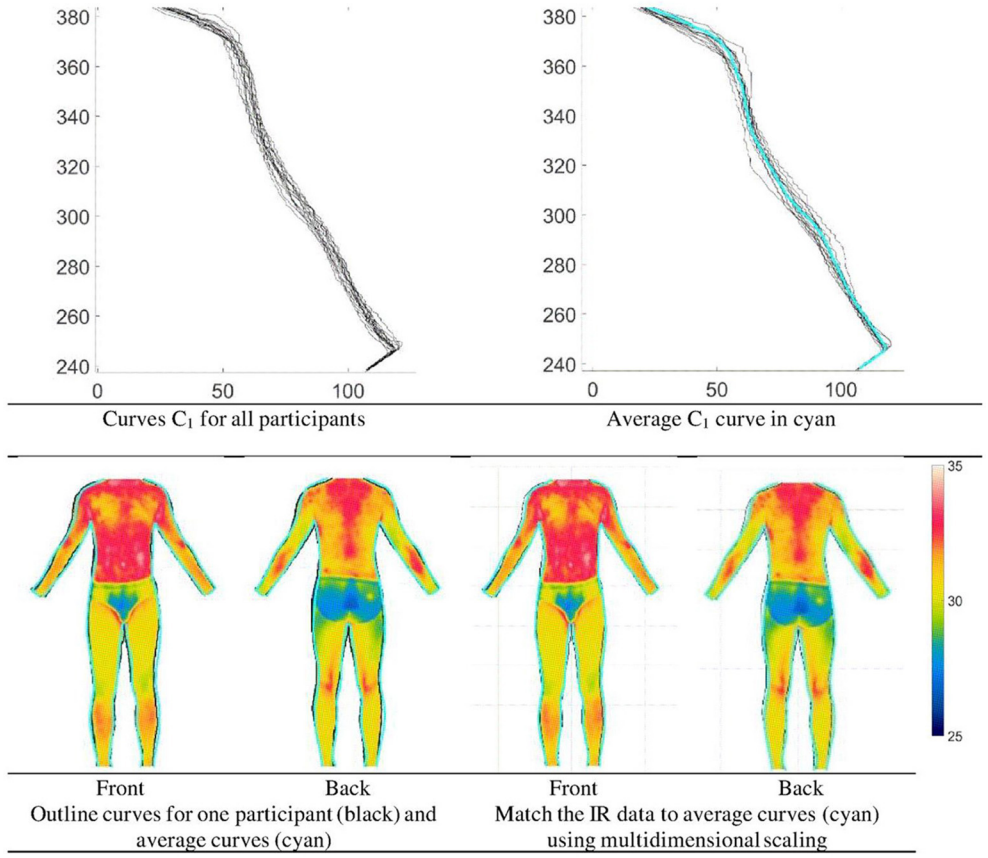

FIGURE 13
Outline curves and multidimensional scaling to match average outline curves (Units: Pixel).

with increasing PC_4 values, the temperature of the upper leg decreases.

Discussion and conclusion

Thermographic study of the human being has been popular for decades. With the advent of high precision InfraRed cameras, the potential for thermographic studies is widespread. Thermography provides a non-intrusive way to provide the state of the internal structure and processes. Changes in the skin surface temperature is an indicator of a person's condition. Recently, Kumar et al. (2022) has provided a review of IR applications in orthopedics and found that IR can provide a form of "heat signature" for medical intervention. With the widespread availability of InfraRed cameras, thermographic studies are finding applications in product design and evaluation (Vitorino et al., 2022). Becerra et al. (2021) have used monitored the hand thermogram when performing repetitive tasks. There are many applications of IR, however the analysis of many studies has been limited to fixed point temperature or subjective evaluations by medical professionals. In this study 4 experiments were carried out to evaluate and quantify the thermogram of human body parts. One of the major contributions in this paper is the use of mathematical model, multidimensional scaling and deformations, image and video analysis using IR data.

When considering the foot, results showed that the average temperature of the foot is higher after wearing socks and shoes for 3 h. Similar situations arise when wearing clothes, protective equipment and even wearables. The average temperature changes and this affects normal body functioning unless the clothing or other wearables match the person's heat dissipation. Such temperature elevations are important because higher temperatures and humid environments are responsible for foot illnesses such as tinea pedis (Luximon et al., 2017).

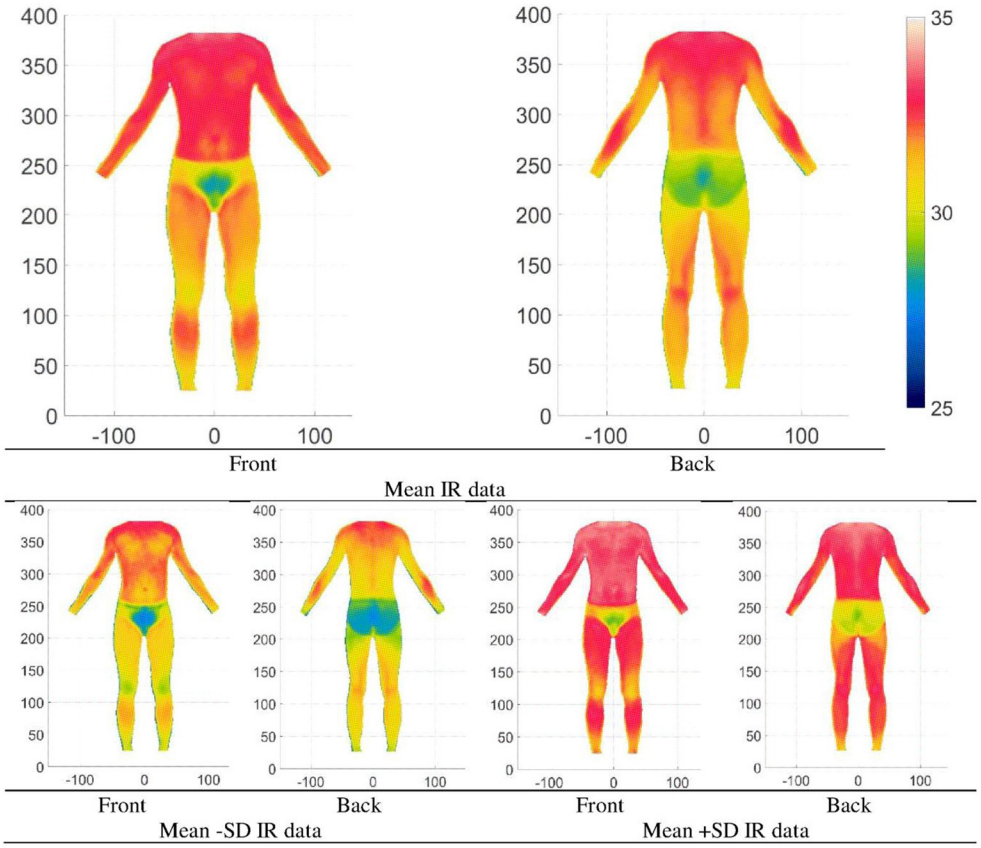

FIGURE 14
Mean and Mean ± SD IR data of whole body-based on all participants (front and back) (Units: Pixel).

With the application of qualitative analysis, IR video data analysis and mathematical trend modeling, we showed the differences in temperature changes at different region of the hand. This method can be used to develop standards for healthy blood flow and medical diagnostics of hand related diseases. Similar techniques can be used to evaluate the blood flow in feet and used for diabetic foot diagnostics.

The study on the whole body showed the use of multidimensional scaling, shear scaling, multidimensional deformation, and averaging techniques to evaluate different body shapes. In addition, the use of principle component analysis showed the main variations in thermograms among population. Four factors represent the variations. From the side of the body, PC_1 represent the variation of hot and cold, PC_2 is somewhat related to the differences between the back of the body and the extremities. PC_3 is somewhat related to the IR distribution of the leg. PC_4 is somewhat related to the IR distribution of the upper arm and leg. When considering from back of the body, PC_1 represent the variation of hot and cold of the whole body. PC_2 is somewhat related to the extremities, especially the leg. PC_3 is somewhat related to the arm and lower leg. PC_4 is somewhat related to the upper leg.

The study of the face and different type of masks showed that the face masks can affect breathing rate. For surgical masks, breathing rate was 10.0 breaths per minute and for N95 masks, breathing rate was 9.7 breaths per minute. For an adult, while resting the normal respiration rate at rest is 12 to 20 breaths per minute and respiration rates of <12 or >25 breaths per minute is considered abnormal (www.healthline.com).

This study illustrates the application of multivariate statistics such as PCA based on IR data. Additionally, application of qualitative analysis, IR video data analysis and mathematical trend modeling based on IR data was also illustrated in this study. The study also illustrated the use of Fourier series modeling in IR data analysis when there is cyclic data. The result of this study has application in the analysis of thermographic data.

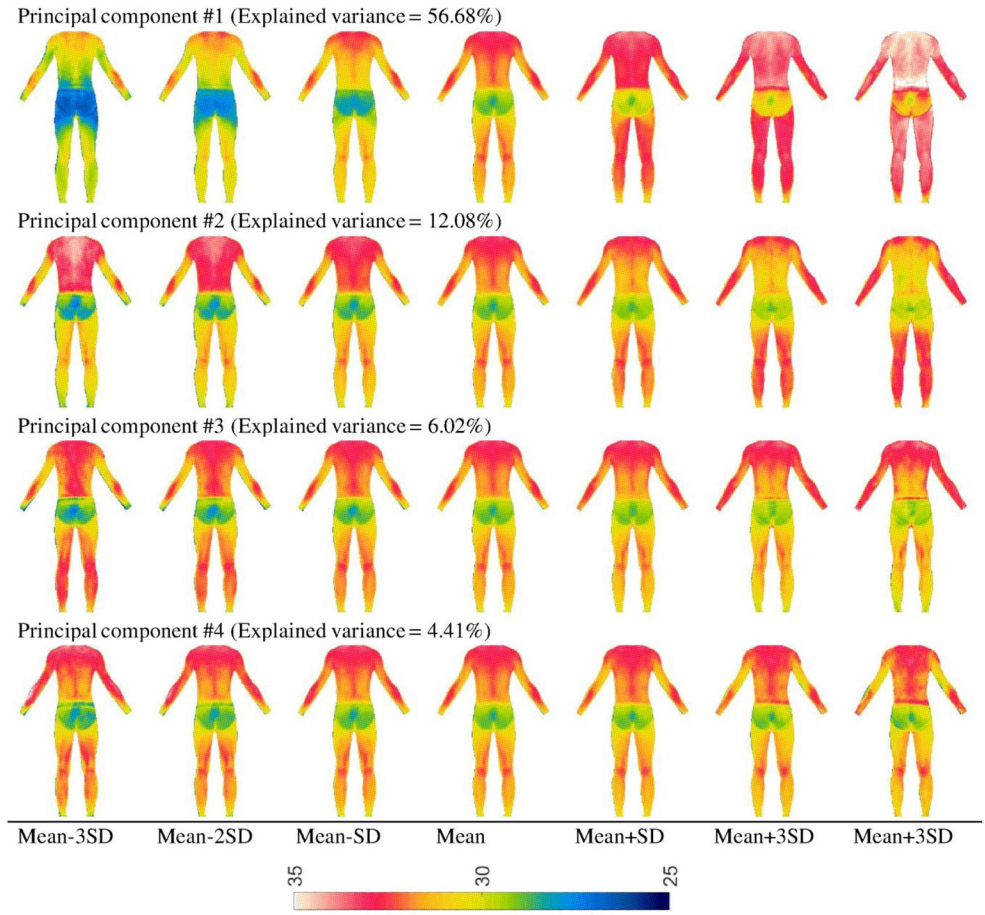

FIGURE 15
Mean and Mean ± SD IR data of whole-body based on all participants (Back) (4 factors explained = 79% variance).

Thermographic data has applications in comparison between groups; classification and grouping; sizing and grading; customization of products; product design, assessment, and evaluations.

Thermography has evolved rapidly these few years and the accuracy of IR cameras has improved while the cost has reduced quite significantly. Although thermography has had its main applications in the medical field, nowadays thermography is being used in a wide range of applications including product design and evaluation and ergonomics. New applications require complex data analysis and data representations and research in this area is needed. Furthermore, with the current pace of development, it seems possible to have an IR camera in our mobile devices. With the widespread use of IR cameras, IR will start to have applications in normal daily life and this will require research in IR data analysis, modeling and visualizations.

There are some limitations in the paper. The sample sizes were not large as the study focus was to explore different analysis methods and its application in the analysis of thermal data, especially time domain data. More studies are needed to create a general model of thermal distribution for the human body and the different body parts. More research is needed for different age group with different Body Mass Index (BMI), gender, and culture in lab as well as field studies.

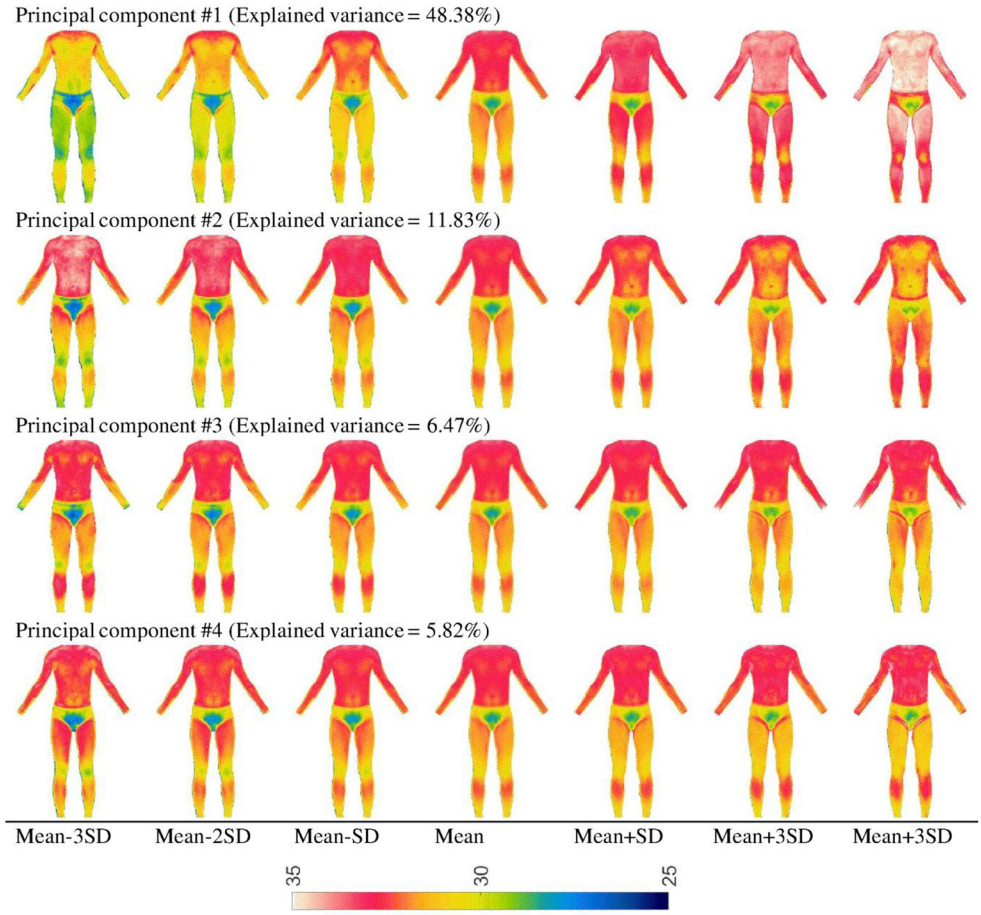

FIGURE 16
Mean and Mean ± SD IR data of whole-body based on all participants (Front) (4 factors explained = 72.5% variance).

Data availability statement

The raw data supporting the conclusions of this article will be made available by the authors, without undue reservation.

Ethics statement

The studies involving human participants were reviewed and approved by the Hong Kong Polytechnic University, Shenzhen University. The patients/participants provided their written informed consent to participate in this study. Written informed consent was obtained from the individual(s) for the publication of any potentially identifiable images or data included in this article.

Author contributions

AL was responsible for the analysis of data, collecting data for Experiment #1, and writing of the paper. HC was responsible for collecting data for Experiment #4 and reviewing the paper. YL was responsible for collecting data for Experiment #2 and #3 and reviewing the paper. RG was responsible for writing the paper, proofreading, and checking the overall analysis. All authors contributed to the article and approved the submitted version.

Funding

This work was financially supported by Guangdong Natural Science Funds for Ph.D. startup Project (2017A030310141).

Acknowledgments

We thank Dr. Balasankar Ganesan and Abida Younus for collecting the data for Experiment #1. Dr. Balasankar Ganesan is a registered physiotherapist and was involved in evaluating the participants.

Conflict of interest

The authors declare that the research was conducted in the absence of any commercial or financial relationships that could be construed as a potential conflict of interest.

Publisher's note

All claims expressed in this article are solely those of the authors and do not necessarily represent those of their affiliated organizations, or those of the publisher, the editors and the reviewers. Any product that may be evaluated in this article, or claim that may be made by its manufacturer, is not guaranteed or endorsed by the publisher.

References

Barcelos, E. Z., Caminhas, W. M., Ribeiro, E., Pimenta, E. M., and Palhares, R. M. (2014). A combined method for segmentation and registration for an advanced and progressive evaluation of thermal images. *Sensors* 14, 21950–21967. doi: 10.3390/s141121950

Becerra, A. G., Olguín-Tiznado, J. E., García Alcaraz, J. L., Camargo Wilson, C., García-Rivera, B. R., Vardasca, R., et al. (2021). Infrared thermal imaging monitoring on hands when performing repetitive tasks: an experimental study. *PLoS ONE* 16, e0250733. doi: 10.1371/journal.pone.0250733

Cade, C. M., and Barlow, B. V. (1967). Fundamental design principles for thermographic scanners. *Sci. Progress* 55:167–185.

Cardone, D., and Merla, A. (2017). New frontiers for applications of thermal infrared imaging devices: computational psychopshysiology in the neurosciences. *Sensors* 17, 1042. doi: 10.3390/s17051042

Chao, H., Luximon, A., and Yeung, K. W. (2015). Functional 3D human model design: a pilot study based on surface anthropometry and infrared thermography. *Comput. Aided Design Applic.* 12, 475–484. doi: 10.1080/16864360.2014.997644

Cruz-Vega, I., Hernandez-Contreras, D., Peregrina-Barreto, H., Rangel-Magdaleno, J. D. J., and Ramirez-Cortes, J. M. (2020). Deep learning classification for diabetic foot thermograms. *Sensors* 20, 1762. doi: 10.3390/s20061762

Drzazga, Z., Binek, M., Pokora, I., and Sadowska-Krepa, E. (2018). A preliminary study on infrared thermal imaging of cross-country skiers and swimmers subjected to endurance exercise. *J. Thermal Anal. Calorimetry* 134, 701–710. doi: 10.1007/s10973-018-7311-y

Faust, O., Acharya, U. R., Ng, E. Y. K., Hong, T. J., and Yu, W. (2014). Application of infrared thermography in computer aided diagnosis. *Infrared Phys. Technol.* 66, 160–175. doi: 10.1016/j.infrared.2014.06.001

Gershon-Cohen, J. (1967). Medical thermography. *J. SMPTE* 76, 1085–1088. doi: 10.5594/J13663

Hildebrandt, C., Raschner, C., and Ammer, K. (2010). An overview of recent application of medical infrared thermography in sports medicine in Austria. *Sensors* 10, 4700–4715. doi: 10.3390/s100504700

Kakileti, S. T., Dalmia, A., and Manjunath, G. (2020). Exploring deep learning networks for tumour segmentation in infrared images. *Quant. Infrared Thermogr. J.* 17, 153–168. doi: 10.1080/17686733.2019.1619355

Kirimtat, A., Krejcar, O., Selamat, A., and Herrera-Viedma, E. (2020). FLIR vs SEEK thermal cameras in biomedicine: comparative diagnosis through infrared thermography. *BMC Bioinformatics* 21, 1–10. doi: 10.1186/s12859-020-3355-7

Kumar, P., Gaurav, A., Rajnish, R. K., Sharma, S., Kumar, V., Aggarwal, S., et al. (2022). Applications of thermal imaging with infrared thermography in Orthopaedics. *J. Clin. Orthopaed. Trauma* 24, 101722. doi: 10.1016/j.jcot.2021.101722

Kwok, G., Yip, J., Yick, K. L., Cheung, M. C., Tse, C. Y., Ng, S. P., et al. (2017). Postural screening for adolescent idiopathic scoliosis with infrared thermography. *Sci. Rep.* 7, 1–8. doi: 10.1038/s41598-017-14556-w

Liu, X., Wang, Y., and Luan, J. (2021). Facial paralysis detection in infrared thermal images using asymmetry analysis of temperature and texture features. *Diagnostics* 11, 2309. doi: 10.3390/diagnostics11122309

Luximon, A., Ganesan, B., and Younus, A. (2017). "Effects of socks and shoes on normal foot skin temperature," in *International Conference on Applied Human Factors and Ergonomics* (Cham: Springer), 485–492. doi: 10.1007/978-3-319-60591-3_44

Luximon, A., and Luximon, Y. (2009). Shoe-last design innovation for better shoe fitting. *Comput. Industry* 60, 621–628. doi: 10.1016/j.compind.2009.05.015

Luximon, Y., Anne Sheen, K., and Luximon, A. (2016). Time dependent infrared thermographic evaluation of facemasks. *Work* 54, 825–835. doi: 10.3233/WOR-162353

Macdonald, A., Petrova, N., Ainarkar, S., Allen, J., Plassmann, P., Whittam, A., et al. (2016). Thermal symmetry of healthy feet: a precursor to a thermal study of diabetic feet prior to skin breakdown. *Physiol. Measur.* 38, 33. doi: 10.1088/1361-6579/38/1/33

Oliveira, J., Vardasca, R., Pimenta, M., Gabriel, J., and Torres, J. (2016). Use of infrared thermography for the diagnosis and grading of sprained ankle injuries. *Infra. Phys. Tech.* 76, 530–541. doi: 10.1016/j.infrared.2016.04.014

Perpetuini, D., Formenti, D., Cardone, D., Filippini, C., and Merla, A. (2021). Regions of interest selection and thermal imaging data analysis in sports and exercise science: a narrative review. *Physiol. Meas.* 42, 8. doi: 10.1088/1361-6579/ac0fbd

Quesada, J. I. P. (ed.) (2017). *Application of Infrared Thermography in Sports Science*. Cham: Springer, 327–327.

Quesada, J. I. P., Kunzler, M. R., and Carpes, F. P. (2017). "Methodological aspects of infrared thermography in human assessment," in *Application of Infrared Thermography in Sports Science* (Cham: Springer), 49–79. doi: 10.1007/978-3-319-47410-6_3

Resmini, R., Silva, L., Araujo, A. S., Medeiros, P., Muchaluat-Saade, D., and Conci, A. (2021). Combining genetic algorithms and SVM for breast cancer diagnosis using infrared thermography. *Sensors* 21, 4802. doi: 10.3390/s21144802

Ring, E. F. J. (2012). History of thermology and thermography: pioneers and progress. *Thermol. Int.* 22.

Skomudek, A., Gilowska, I., Jasiński, R., and Rozek-Piechura, K. (2017). Analysis of the dynamics of venous blood flow in the context of lower limb temperature distribution and tissue composition in the elderly. *Clin. Interv. Aging.* 12, 1371. doi: 10.2147/CIA.S137707

Stade, E. (2011). *Fourier Analysis*. Hoboken, NJ: John Wiley and Sons.

Timm, N. H. (ed.) (2002). *Applied Multivariate Analysis*. New York, NY: Springer New York.

van Doremalen, R. F., van Netten, J. J., van Baal, J. G., Vollenbroek-Hutten, M. M., and van der Heijden, F. (2020). Infrared 3D thermography for inflammation detection in diabetic foot disease: a proof of concept. *J. Diabetes Sci. Technol.* 14, 46–54. doi: 10.1177/1932296819854062

Vitorino, D. F., Soares, M. M., and Marçal, M. A. (2022). "Applications of infrared thermography to evaluate the ergonomics and usability of products with a gestural interface," in *Handbook of Usability and User Experience* (Boca Raton, FL: CRC Press), 301–330. doi: 10.1201/9780429343490-22